Design of Multiband Baluns on Liquid Crystalline Polymer (LCP) Based Substrates

Vinu Govind*, Sidharth Dalmia, Venky Sundaram, George E. White and Madhavan Swaminathan**
Georgia Institute of Technology
School of Electrical and Computer Engineering
Atlanta, GA 30332, USA.
*vgovind@ece.gatech.edu, **madhavan.swaminathan@ece.gatech.edu

Abstract

Baluns operating at multiple frequency bands can result in a reduction in the size of multiband RF front-ends. This paper presents novel multiband balun topologies, using both distributed as well as lumped components. Using LCP packaging technology, baluns operating simultaneously at the 930 and 2000 MHz frequency bands have been fabricated. Measurements show –14.5 dB and –32.4 return loss in the lower and upper bands. The phase and amplitude imbalances are less than 2.5° and 0.6 dB in each band.

I. Introduction

With a proliferation of wireless standards and applications, the need for RF front-ends that support multiple bands and multiple protocols becomes necessary. E.g., A WLAN device supporting 802.11a/b/g protocols (2.4 GHz and 5.2 GHz), or a cell phone supporting GSM900, DCS1800 and PCS1900 protocols (900 MHz, 1800 MHz and 1900 MHz). However, simply stacking multiple receiver chains each operating at a different frequency results in large form-factor and high power consumption for these devices. As mobile applications (where small size and low power consumption are very important) constitute a large percentage of the wireless market, making the individual RF components functional at multiple frequencies become necessary to keep form-factor and power consumption under control [1].

Baluns are three-port devices that provide balanced outputs from unbalanced inputs, and are key components in most RF front-ends [2]. With the move towards miniaturization, they need to be compact as well as functional at multiple frequency bands, to meet the space constraints of modern multiband wireless systems. However, traditional implementations of baluns using transmission line elements occupy large areas, and smaller devices (by the use of purely lumped element designs or by transmission line size reduction schemes with the use of lumped capacitors) are limited by the additional cost of these discrete components.

Developments in packaging technology have resulted in the System-On-Package (SOP) approach emerging as an important means for integration of RF front-ends. Low loss materials like Liquid Crystalline Polymer (LCP) allow the implementation of high-Q passives in the packaging substrate, which allows the designer to achieve completely integrated and compact balun solutions without the use of discrete passives.

The major contributions of this paper are as follows:

1) This paper describes the analysis and design of compact concurrent multiband baluns. The devices are implemented through two topologies, one using a combination of distributed and lumped elements, and another using purely lumped components.
2) This paper also presents, for the first time, baluns fabricated on an LCP substrate. The devices have been realized through the use of embedded high-Q passives, and are thus completely integrated. Further, they provide the possibility of a completely integrated RF front-end through SOP based implementation schemes.

This paper is organized as follows: Section II describes possible multiband transceiver architectures while Section III covers the design and analysis of three multiband balun topologies. Section IV includes information on the LCP process used to fabricate the devices, and measurement results. This is followed by Section V, which analyses the results and provides conclusions.

II. Multiband Architectures

Multiband operation can be achieved in the following ways: 1) Systems with wide bandwidths capable of operating at different frequency bands 2) Narrow-band devices that switch between frequency bands (sampling only a single frequency at any given time) [3] or 3) concurrent devices that achieve simultaneous multiband functionality (sampling one or more frequencies at a time depending on application) [1]. Of these, option 1 is difficult to implement due to

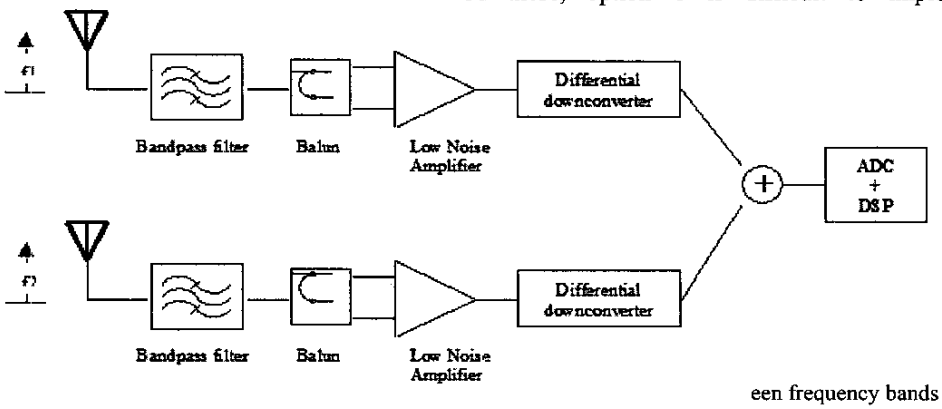

Fi

een frequency bands in the baseband

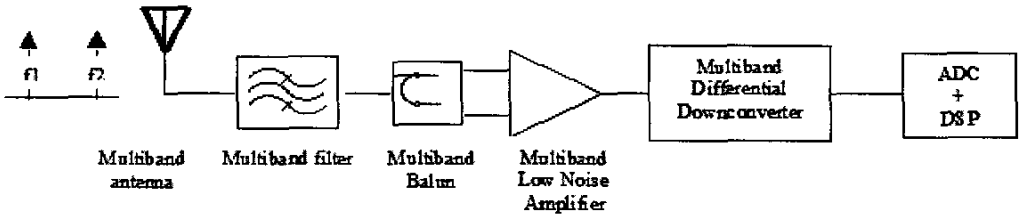

Fig 2. Concurrent multiband architecture, with each component functional at multiple frequency bands

technological concerns and due to the presence of large blocker signals close to the frequency bands of interest.

Option 2 can be achieved by stacking multiple single-frequency RF front-ends together, and then switching between them (Fig. 1). However, this results in large sizes and high power consumption. In contrast, the use of multiband devices can lead to low power consumption and a vastly reduced footprint. Fig. 2 shows such a concurrent architecture, where each device is functional at multiple frequency bands. Depending on the application, this results in the sampling of single or multiple frequencies at any given time. For e.g., a cell phone supporting multiple standards can choose to receive a signal at 900 MHz, 1.9 GHz or 2.1 GHz, depending on area of coverage and type of service. Similarly, a GSM900 cell phone with WLAN capabilities can simultaneously communicate with the base-station (at 900 MHz) as well as receive signals from the WLAN router (at 2.4 GHz).

III. Multiband Balun Analysis

The key function of a balun is to transform unbalanced inputs to a balanced output. In terms of S parameters of the device, this results in the following conditions [4]:

$$S11 = 0;\ S21 = -S31 \qquad (1)$$

Several papers have described the design of baluns using distributed or lumped elements, or a combination of both [4]-[6]. However, these examples are single-band devices, and often focused on the reduction in device size.

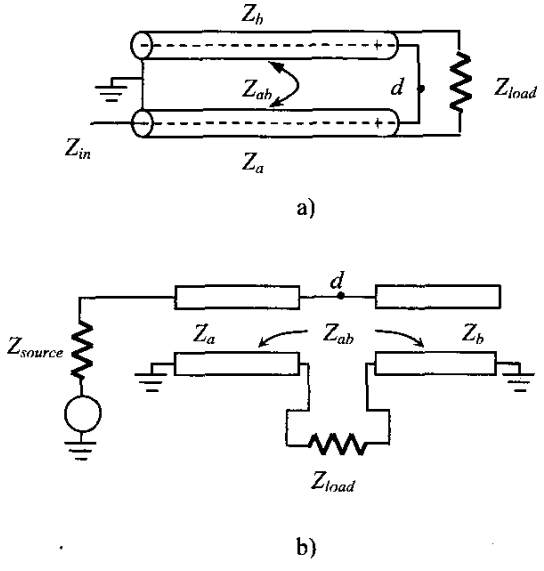

Fig 3. a) Coaxial balun b) Simplified schematic

A) Topology 1: Transmission Line Implementation:

Fig. 3 shows the simplified schematic of a Marchand balun ([6], [2]). The input impedance seen at d has been derived as [6]

$$Z_d = \frac{Z_{load}}{\frac{Z_{load}^2}{Z_{ab}^2 \tan^2\theta}+1} + \frac{jZ_{load}^2 Z_{ab}\tan\theta}{Z_{load}^2 + Z_{ab}^2\tan^2\theta} - jZ_b\cot\theta \qquad (2)$$

where θ is the electrical length of the transmission line segments, and the rest of the variables are as shown in Fig. 3.

The impedance seen by the source (Z_{in}) can then be calculated by transforming Z_d with a length of transmission line with characteristic impedance Z_a.

$$Z_{in} = Z_a \frac{Z_d + jZ_a\tan\theta}{Z_a + jZ_d\tan\theta} \qquad (3)$$

assuming lossless operation.

The input return loss $S11$ is thus a function of Z_a, Z_b, Z_{ab}, Z_{load}, Z_{source} and θ. Perfect matching ($\mathrm{Im}(Z_{in}) = 0$ and $\mathrm{Re}(Z_{in}) = Z_{source}$, leading to $S11 = 0$) occurs when Z_a is set equal to $(Z_{source}.Z_{load})^{1/2}$ and the lengths of the transmission line segments are chosen such that $\theta = 90°$. However, it has been shown in [7] that a perfect input match can be achieved at two angles θ_1 and θ_2, by setting:

$$Z_{ab} = Z_{load}, \qquad Z_a = Z_b = Z_{load}\sin^2\theta_{1,2} \qquad (4)$$

θ_1 and θ_2 are obtained by the input/output impedance ratios, and lie symmetrically above and below 90° [6]. The input match at the band-center (corresponding to $\theta = 90°$) is reduced as a result, but the $S11$ is still less than -15 dB, meeting most specifications.

θ_1 and θ_2 are functions of frequency, and are given by:

$$\theta_1 = \frac{\pi}{2}\frac{f_1}{f_0} \qquad \theta_2 = \frac{\pi}{2}\frac{f_2}{f_0} \qquad (5)$$

where f_0 is the frequency corresponding to 90°. It can thus be seen that by extending this analysis further, it is possible to create baluns that are simultaneously functional at *any* two different frequencies f_1 and f_2, by choosing appropriate values for Z_a, Z_b, Z_{ab}, Z_{load} and Z_{in}.

Both [6] and [7] have used examples where θ_1 and θ_2 are obtained above and below 90° by using $Z_{load} \neq Z_{source}$. However, the source and load impedances are usually set by system requirements, and are beyond the control of the balun designer. Setting Z_a different from Z_b offers the designer an extra degree of freedom, and makes it possible to make the frequencies of operation independent of the load and source impedances. (This also results in the degradation of the input

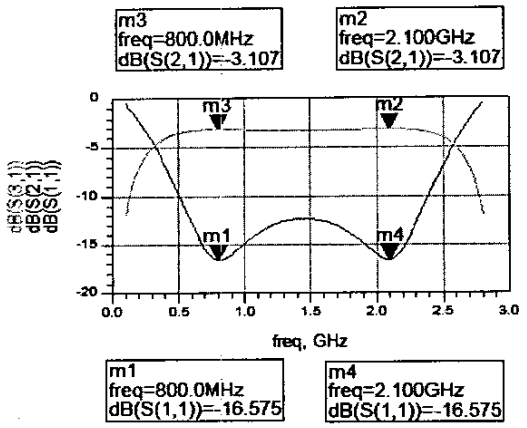

Fig 4. S-parameter simulation of the balun (Topology 1), showing input match (S11) and power loss (S21 and S31) in the 800 MHz and 2.1 GHz frequency bands.

match at the center frequency f_0. However, as the applications are usually narrow band in nature, the low *S11* obtained at the two frequencies f_1 and f_2 are sufficient to make the balun functional).

As an example, a balun operating at both 900 MHz and 1.9 GHz with source and load impedances of 50Ω each was designed using the above methodology. The center frequency was chosen to be 1.45 GHz. Using (4), this yields values of 50Ω and 29.045Ω for Z_{ab} and Z_b respectively. By choosing Z_a = 64Ω, *S11* is obtained to be -16.575 dB at 800 MHz and 2.1 GHz. The *S11* at the center frequency (1.45 GHz) is -12.32 dB. Fig. 4 shows the simulation (HP-ADS™) results of the device.

B) Topology 2: Distributed-Lumped Implementation:

In the previous example, transmission line segments with $\theta = 90^\circ$ at 1.45 GHz were used to obtain balun functionality at 800 MHz and 2.1 GHz (with equal bandwidths at each center frequency). With the use of capacitive loading, the physical size of these segments can be brought down further [4]. However, this also leads to a narrowing of bandwidths.

In several dual-band applications, it is important to have a control over the individual bandwidth as well. For e.g., a WLAN access device supporting the 802.11a/b/g protocols requires a 100 MHz bandwidth centered around 2.44 GHz (for 802.11b/g) while a 1 GHz bandwidth centered around 5.4 GHz is required for 802.11a.

Fig. 5 shows the schematic of a novel dual band balun. The device has a basic Marchand topology, but adds a frequency dependent imaginary impedance X (by way of inductors or capacitors) in series with the output load Z_{source}.

Equation (2) can re-derived for the new topology as:

$$\mathrm{Re}(Z_d) = \frac{Z_{load} Z_{ab}^2 \tan^2\theta}{Z_{load}^2 + (X + Z_{ab}\tan\theta)^2} \qquad (6a)$$

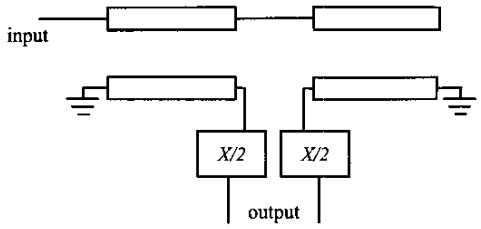

Fig 5. Schematic of the new balun, with two frequency dependent impedances (X/2) added in series with the load.

$$\mathrm{Im}(Z_d) = \frac{Z_{ab}\tan\theta(Z_{load}^2 + X^2 + XZ_{ab}\tan\theta)}{Z_{load}^2 + (X + Z_{ab}\tan\theta)^2} - Z_b\cot\theta \qquad (6b)$$

The use of the two extra components gives an extra degree of freedom to the designer, which can be used to control the operation of the balun at different frequencies. The element X has the effect of scaling the load impedance seen by the balun. As in the previous design, Z_{in} has real and imaginary components at both frequency bands; this reduces the power transfer to the load, which appears as an increase of power loss in the balun. However, the reflection is small and the extra loss can be tolerated in a number of applications, especially those involving short-distance communication protocols.

It is to be noted that the use of inductors or capacitors in series with the load changes the electrical length of the transmission line segments. Inductors result in electrically shorter devices, which requires an increase in the physical size of the device. Capacitors on the other hand lead to an increase of electrical lengths, effectively reducing the physical size of the device. Capacitive loading of the transmission line segments can be done independent of the load elements used, leading to further reductions in device size.

As a design example, a balun for a WLAN receiver using the 802.11a/b/g protocols was designed. The frequencies of operation were 2.4 GHz (with a 100 MHz bandwidth) and 5.4 GHz (with 1 GHz bandwidth). The source and load impedances were 50Ω and 100Ω respectively. Using the design methodology described above, values for even-mode and odd-mode impedances of the transmission line segments were fixed at 85Ω and 25Ω respectively. Two capacitors of 1.25 pF each were used to provide the value of X in equation (6). Due to capacitive loading, the electrical lengths of the lines increased, which resulted in a reduction in physical length of the device – instead of 90°, a θ of 75° (at 3.9 GHz, the frequency midway between the bands) was used. Fig. 6 shows the simulation (HP-ADS™) results of the device.

The new design has the effect of increasing component count. However, a key feature of SOP based integration schemes is that the *number* of lumped components is less important than the *value* of each of these components, as all the components can be embedded in the package, but larger component values result in larger device sizes. (In contrast, designs utilizing discrete passives are more concerned with

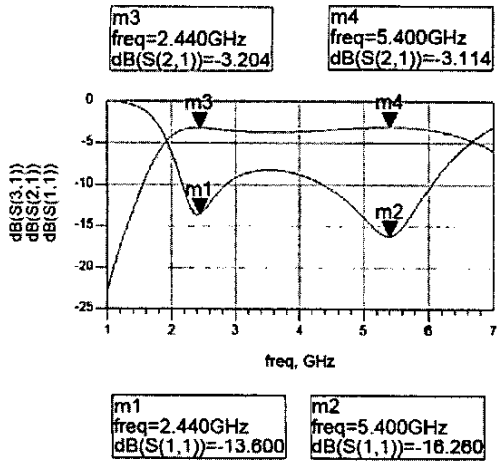

Fig 6. S-parameter simulation of the balun (Topology 2), showing input match (S11) and power loss (S21 and S31) in the 2.44 GHz and 5.4 GHz frequency bands.

the total number of passives and not the individual values of each; the cost of assembly depends only on the numbers of discrete elements to be soldered on board, and the packaged size for different values of capacitance or inductance remains the same for a commercially available discrete device).

C) Topology 3: Lumped Circuit Implementation:

With materials were the dielectric constant is low (as with many commercially available low-loss organic technologies), designs involving transmission lines tend to occupy large areas. In such scenarios, lumped element balun implementations using embedded passives result in devices with small form factor.

Lattice type baluns such as the one shown in Fig. 7 are ideal for narrowband applications such as 802.11b/g where the operating frequency is 2.45GHz ± 50MHz; for larger bandwidth applications such as 802.11a where the operating frequency is 5.4 ± 500MHz the schematic shown in Fig. 8 can be used.

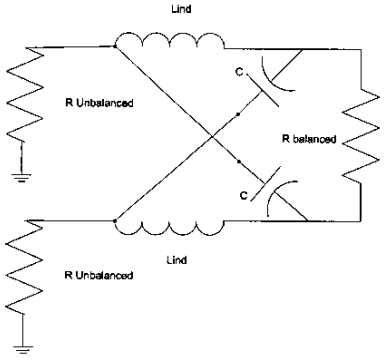

Fig 7. Lattice type balun used for the implementation of narrowband application

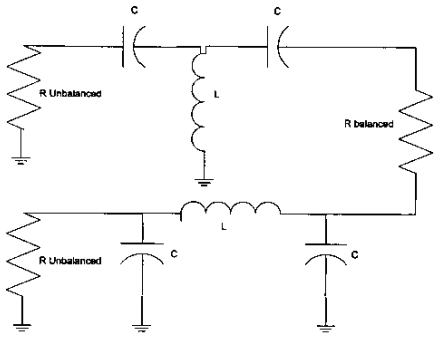

Fig 8. Broadband lumped element type balun used for the implementation of narrowband application

The data for single band baluns has been shown in [8], (which is being presented at the same venue as this paper) and will not be repeated here.

Single band baluns can be modified for multiband functionality, by using series and parallel resonant circuits in place of the capacitors and inductors in the circuits of Fig. 7 and 8 respectively. The balun circuit of Fig. 8, modified to achieve multiband functionality, is shown in Fig. 9. The values for circuit elements have been calculated for simultaneous balun operation at 2.4GHz and 5.5GHz.

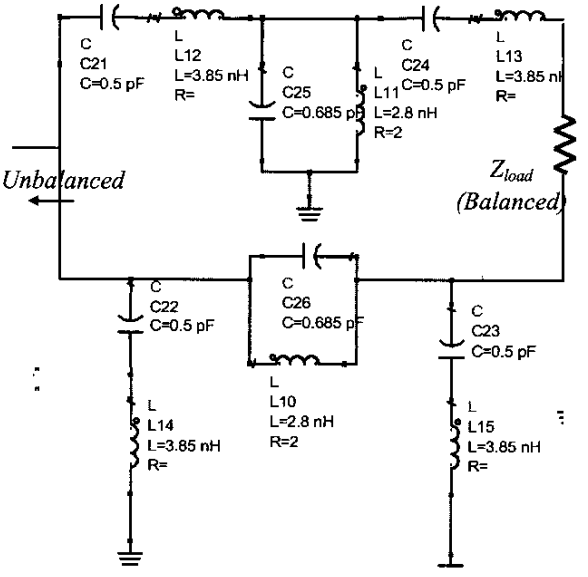

Fig 9. A 2.4/5.5 GHz multiband balun used for transformation of 75 ohm balanced load to 75 ohm unbalanced source

Fig. 10 shows post-layout simulated data (using Sonnet™) for the fully packaged balun shown in Fig. 9. The simulation data shows a narrowband of operation at 2.45GHz±150MHz with an amplitude imbalance of ±0.6dB and phase imbalance of ±5 degrees within the band. Compared to the lower band, the balun shows a broader band of operation at 5.5GHz ±

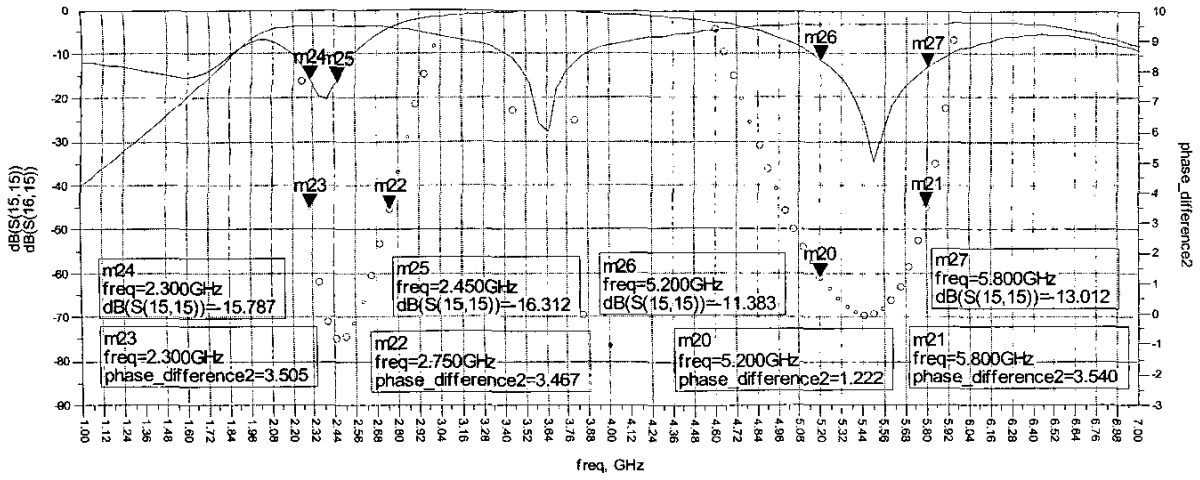

Fig 10. Post-layout simulated data (using Sonnet™), for the fully packaged balun of Fig. 9.

300Mhz with an amplitude imbalance of ±0.6dB and phase imbalance of ±5 degrees within the band. This balun, fully packaged, measured 2mm x 3.5mm x 1.5mm. It is important to note that the bandwidth in each band can be altered by changing the resonant frequency of the series and parallel LC pairs used in Fig. 9. In this example, the desired resonant frequency for each of these sections was ~ 3.5GHz.

IV. Design, Fabrication, Measurements and Analysis

A 3-metal layer organic process was used for the fabrication of the devices. It consisted of a 1-mil diclad low loss laminate, LCP, ($\tan\delta = 0.002$, $\varepsilon_r = 2.95$) laminated onto a low loss core layer that is 30 mils thick. The ability to use thin layers with low loss tangent and microvia technology helps achieve capacitor and inductor Qs greater than 200 in a small area.

A Topology 2 balun for use at 930MHz and 2130 MHz was designed for the above LCP process. The source and load impedances were 50Ω and 100Ω respectively. The design methodology of Section IV resulted in odd-mode and even mode impedances of 25Ω and 110Ω respectively. Two capacitors of 3.5 pF each were used in series with the load impedance to make the balun functional at both frequencies. To further reduce the size of the device, capacitive loading was employed with the use of four more embedded capacitors (each 2.5 pF in value). This resulted in the physical length of the transmission line segments being ~λ/10 (or $\theta = 35^{\circ}$) at 1.53 GHz (the frequency midway between 930 MHz and 2130 MHz).

The coupled line segments were implemented as edge-coupled devices, with the required values of odd and even mode impedances achieved by placing each line of a coupled line pair in different metal layers. Coiling during layout resulted in a reduction in the required physical length of the transmission line segments, from ~λ/10 to ~λ/11 at 1.53 GHz. Fig. 11 shows the photograph of the fabricated balun. The device measures 1.5 cm x 0.6 cm, including CPW ground rings and probe pads.

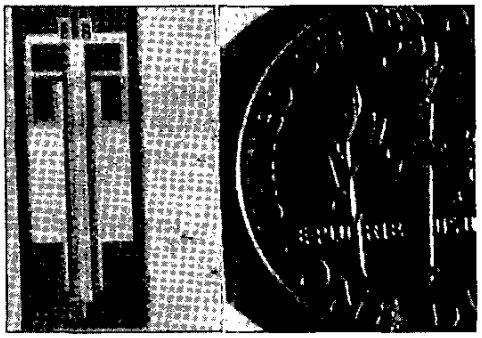

Fig 11. Photograph of the balun fabricated on an LCP substrate. The device measures 1.5 cm x 0.6 cm, including the CPW ground rings and probe-pads.

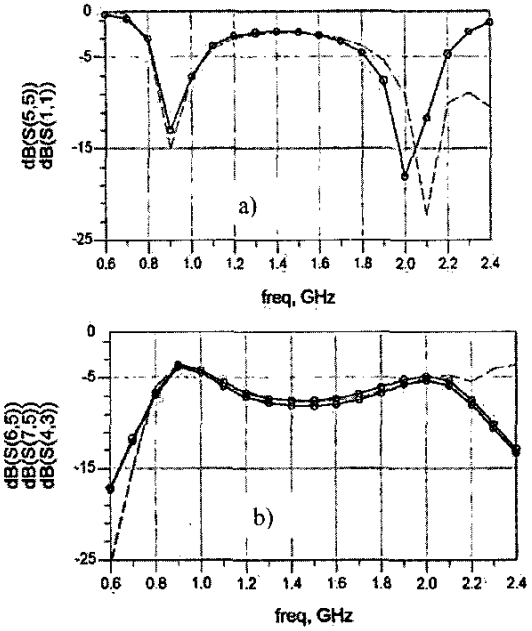

Fig 12. Simulated (Sonnet) and measured results for the fabricated balun a) Input match (S11) b) Power transfer (S21 and S31). Solid line with dots represent measured values, dashed line represents simulated results.

Author	Frequency	Area	Material
Ang et al. [4]	1.1GHz-1.6GHz	1cm x 1cm	er = 4.5
Kumar et al. [9][1]	1.9 GHz	Not given	er = 4.1
Raicu et al. [10]	2.1GHz-3.6GHz	7.5cm x 4.9cm	er = 2.2
This work	890MHz-960MHz & 1.95GHz-2.11GHz	1.5cm x 0.6cm	er=2.95

Table 2. Comparison of current work with others. ([1]The bandwidth of operation was not mentioned in the paper. The size of the transmission line segments was given to be ~λ/16, however the size of the layout was not given).

Fig. 12 shows the measured values for *S11*, *S21* and *S31*, along with post-layout full-wave simulation results (Sonnet™). The amplitude and phase balance over the frequency range of interest is shown in Fig. 13.

The measured *S11* dips to -14.5 dB at 920 MHz. However, the upper band exhibits a downward shift in frequency, with *S11* reaching a minimum of -32.4 dB at 2.03 GHz rather than the 2.13 GHz it was designed to be at. A small shift in layer-to-layer alignment during fabrication contributed to this frequency shift. The loss, which is less than a dB in the lower frequency band increases beyond 1 dB for the upper band. This is due to significant back coupling between the output capacitors and the coupled line segments, as a need to keep device size minimum resulted in a very compact layout. The phase difference remains less than a degree in the lower band, and increases to a maximum of 2.5° in the upper band. The amplitude imbalance is less than 0.25 dB in the lower band while it increases to a maximum of 0.6 dB in the upper band. Table 1 summarizes the measurement results for the balun.

Table 2 shows a performance comparison of the new device with other distributed and lumped-distributed baluns fabricated on materials with comparable dielectric constants. Balun performance is dependant on source and load impedances, and its size depends on the layout; however, it can still be observed that there is a clear tradeoff between bandwidth and device size. Though it can be argued that examples like [9] with large bandwidths can be used at multiple frequency bands, this also results in large device sizes. A reduction in size by the use of capacitive loading [4] results in smaller size, but the bandwidth of operation too becomes narrow preventing operation at multiple frequencies. The new topology allows the simultaneous optimization of size and multiband functionality, while exhibiting good amplitude and phase balance in the frequency bands of interest. It results in compact baluns, at the same time allowing control over bandwidths at frequencies of interest.

The size of devices with distributed elements is dependant on the dielectric constant of the substrate material used. The device of [11] is thus very small, due to the high dielectric constant offered by the ceramic process. The topologies presented in this paper would also benefit from a fabrication process with a higher dielectric constant, and it is possible to have a size reduction of up to three times by moving to a ceramic process, while still meeting the criterion of controlled multiband operation.

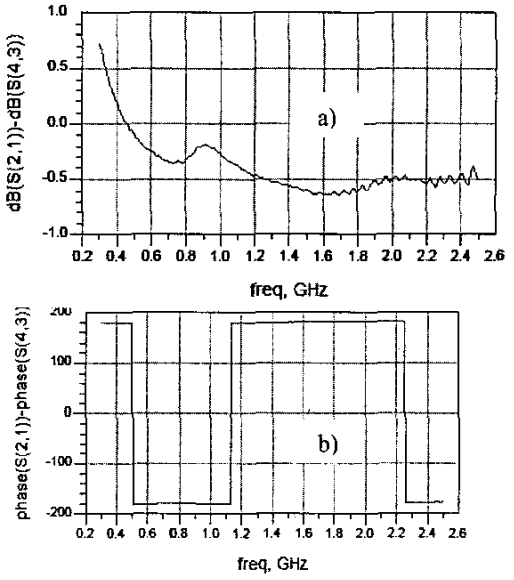

Fig 13. Measured amplitude imbalance (a) and phase imbalance (b) for the balun.

	920 MHz	2.03 Ghz
Bandwidth	70 MHz	160 MHz
S11	-14.5 dB	-32.4 dB
S21	-3.54 dB	-4.93 dB
S31	-3.73 dB	-5.35 dB
Amplitude Imbalance	0.19 dB	0.42 dB
Phase Imbalance	0.73 deg	1.9 deg

Table 1. Measured performance of the balun.

V. Conclusions

Design methodologies for different multiband balun implementations on LCP substrates have been presented for the first time. Designs for baluns using purely lumped components as well as a combination of lumped and distributed elements have been described.

A novel balun topology, with simultaneous optimization of size, bandwidth and multiband functionality has been proposed. The new device uses a Marchand balun as the core

circuit, along with output impedance scaling. Embedded passives are used to achieve the impedance scaling, which results in optimized and controllable multiband functionality for the balun. Equations have been developed for the design of these networks using embedded passives. Capacitive loading has also been applied to reduce the size. The main advantage of the new design is a reduction in size through increased functionality; compared to a standard Marchand balun that requires two $\lambda/4$ segments of coupled lines and operates at only one frequency, the new design uses two $\lambda/18$ segments at 930 MHz - and manages to make the balun functional at 2 GHz as well.

The examples have been designed for a multi layer LCP process; however, the design equations are valid for a variety of processing technologies, and depending on material properties, one or the other design can be chosen for implementation. These devices will play a key role in the development of compact multiband multi-standard RF front-ends.

Acknowledgments

The authors wish to acknowledge the assistance received from Jacket Micro Devices, Inc., Atlanta, in the fabrication of the devices.

References

1. H. Hashemi and A. Hajimiri, "Concurrent multiband low-noise amplifiers - theory, design and applications", *IEEE Transactions on Microwave Theory and Techniques*, vol. 50, pp. 288-301, Jan. 2002.
2. Y. J. Yoon, Y. Lu, R. C. Frye and P. R. Smith, "Spiral transmission-line baluns for RF multichip module packages", *IEEE Transactions on Advanced Packaging*, vol. 22, pp. 332-336, Aug. 1999.
3. S. Wu and B. Razavi, "A 900-MHz/1.8-Ghz CMOS receiver for dual-band applications", *IEEE Journal of Solid-State Circuits*, vol. 33, pp. 2178-2185, Dec. 1998.
4. K. S. Ang, Y. C. Leong and C. H. Lee, "Analysis and design of miniaturized lumped-distributed impedance-transforming baluns", *IEEE Transactions on Microwave Theory and Techniques*, vol. 51, pp. 1009-1017, March 2003.
5. D. -W. Lew, J. -S. Park, D. Ahn, N. -K. Ahn, C. S. Yoo and J. -B. Lim, "A design of the ceramic chip balun using the multilayer configuration", *IEEE Transactions on Microwave Theory and Techniques*, vol. 49, pp. 220-224, Jan. 2001.
6. W. K. Roberts, "A new wide-band balun", Proceedings of the IRE, vol. 45, pp. 1628-1631, Dec. 1957.
7. J. -W. Lee and K. J. Webb, "Analysis and design of low-loss planar microwave baluns having three symmetric coupled lines", *IEEE MTT-S International Microwave Symposium Digest*, pp. 117-120, June 2002.
8. S. Dalmia, V. Sundaram, G. White and M. Swaminathan, "Liquid Crystalline Polymer based RF/wireless components for multi-band applications", accepted for presentation at the *IEEE Electronic Components and Technology Conference (ECTC)*, May 2004.
9. B. P. Kumar and G. R. Branner, "Optimized design of unique miniaturized planar baluns for wireless applications", *IEEE Microwave and Wireless Components Letters*, vol. 13, pp134-136, Feb. 2003.
10. D. Raicu, "Design of planar, single-layer microwave baluns", *IEEE MTT-S International Microwave Symposium Digest*, pp. 801-804, June 1998.
11. C. -W. Tang, J. -W. Sheen and C. -Y. Chang, "Chip-type LTCC-MLC baluns using the stepped impedance method", *IEEE Transactions on Microwave Theory and Techniques*, vol. 49, pp. 2342-2349, Dec. 2001.